The Astrophysical Journal, 785:31 (7pp), 2014 April 10 doi:10.1088/0004-637X/785/1/31

DETAILED NUMERICAL INVESTIGATION OF THE BOHM LIMIT IN COSMIC RAY DIFFUSION THEORY

M. Hussein and A. Shalchi
Department of Physics and Astronomy, University of Manitoba, Winnipeg, Manitoba R3T 2N2, Canada; m_hussein@physics.umanitoba.ca, andreasm4@yahoo.com
Received 2013 December 22; accepted 2014 February 13; published 2014 March 21

ABSTRACT

A standard model in cosmic ray diffusion theory is the so-called Bohm limit in which the particle mean free path is assumed to be equal to the Larmor radius. This type of diffusion is often employed to model the propagation and acceleration of energetic particles. However, recent analytical and numerical work has shown that standard Bohm diffusion is not realistic. In the present paper, we perform test-particle simulations to explore particle diffusion in the strong turbulence limit in which the wave field is much stronger than the mean magnetic field. We show that there is indeed a lower limit of the particle mean free path along the mean field. In this limit, the mean free path is directly proportional to the unperturbed Larmor radius like in the traditional Bohm limit, but it is reduced by the factor $\delta B/B_0$ where B_0 is the mean field and δB the turbulent field. Although we focus on parallel diffusion, we also explore diffusion across the mean field in the strong turbulence limit.

Key words: diffusion – magnetic fields – turbulence

1. INTRODUCTION

Cosmic rays propagate in turbulent plasmas in different astrophysical scenarios ranging from the solar system to the intergalactic space. In all such systems one finds a large scale or mean magnetic field that is superposed by a turbulent component that is often associated with propagating plasma waves and, thus, the component is often called the wave field. Therefore, we can write the total magnetic field as $\boldsymbol{B} = B_0\boldsymbol{e}_z + \delta\boldsymbol{B}$, where we have chosen our Cartesian system of coordinates so that the mean field $\boldsymbol{B}_0$ points in the z-direction. The aforementioned mean field alone would only force the particles onto a well-defined trajectory that would correspond to a *helix*. In this particular case, which is often referred to as the *unperturbed system*, the particles move with constant speed along the mean field while the perpendicular motion is a uniform circular motion. The unperturbed motion can easily be derived analytically from the *Newton–Lorentz equation*. In this case, the characteristic quantities used to describe the orbit are the particle speed v, pitch-angle cosine $\mu = v_\parallel/v$, and gyro-frequency Ω, which can be expressed by $\Omega = qB_0/(mc\gamma)$. In the latter formula we have used the particle charge q, particle rest mass m, speed of light c, and *Lorentz factor* γ.

However, there is turbulence in real physical scenarios—such turbulent magnetic fields scatter the energetic particles and particle motion becomes a diffusive motion described by diffusion parameters. Therefore, in order to compute cosmic ray distribution functions, a diffusive transport equation has to be solved. The following is an example of a transport equation (see, e.g., Schlickeiser 2002):

$$\frac{\partial f}{\partial t} - S(\boldsymbol{x},\boldsymbol{p},t) = \frac{\partial}{\partial z}\left[\kappa_{zz}\frac{\partial f}{\partial z}\right] - \frac{1}{4p^2}\frac{\partial(p^2vD)}{\partial p}\frac{\partial f}{\partial z} + \sum_{i,j=x,y}\frac{\partial}{\partial x_i}\left[\kappa_{ij}\frac{\partial f}{\partial x_j}\right] + \frac{1}{p^2}\frac{\partial}{\partial p}\left(p^2A\frac{\partial f}{\partial p}\right) + \frac{v}{4}\frac{\partial D}{\partial z}\frac{\partial f}{\partial p}. \quad (1)$$

In the latter equation we used the parallel diffusion coefficient $\kappa_\parallel \equiv \kappa_{zz}$, the perpendicular diffusion coefficients κ_{ij}, the rate of adiabatic deceleration D, and the momentum diffusion coefficient A describing stochastic acceleration. More complicated forms of the transport equation can be found in the literature. There are cases, for instance, in which the assumption of a constant mean field is no longer valid and the so-called adiabatic focusing has to be taken into account leading to a modified equation (see Schlickeiser et al. 2007). In all forms of the transport equation, there are at least two crucial transport parameters, namely the parallel spatial diffusion coefficient $\kappa_\parallel$ and the perpendicular diffusion coefficient $\kappa_\perp$ (in axi-symmetric scenarios only the parameter $\kappa_\perp \equiv \kappa_{xx} \equiv \kappa_{yy}$ controls the perpendicular diffusion term in the transport equation).

Obviously, parallel and perpendicular diffusion coefficients have to be known in order to describe the motion of cosmic rays. In principle there are two methods to estimate these parameters. The first approach is analytical theory. Early work was based on perturbation theory, also known as quasi-linear theory, which was originally developed by Jokipii (1966). Although the latter work was pioneering and is still important in current applications, quasi-linear theory has its limitations (see Shalchi 2009a for a review). Therefore, nonlinear methods were developed to achieve a more complete and accurate description of cosmic ray transport (see, e.g., Shalchi 2009a, 2010). The perturbation theory is thought to be valid in the weak turbulence limit in which the true particle orbit is close to the unperturbed trajectory. Very strong turbulence, in which the wave field is much stronger than the mean field $\delta B \gg B_0$, is another extreme limit. In this particular case it is often assumed that, the so-called *Bohm limit* is found, where by definition

$$\lambda \sim R_L \qquad \textit{(Standard Bohm Limit)}, \quad (2)$$

where we used the unperturbed Larmor radius R_L and the (isotropic) particle mean free path $\lambda = 3\kappa/v$. We refer to Equation (2) as the *standard Bohm limit*. This limit is questionable, however, because in real physical scenarios particles experience strong scattering, and a well-defined gyro-rotation can no longer be found (see, for example, Figure 2 of Giacalone & Jokipii 1999).

Shalchi (2009b) used methods of nonlinear diffusion theory to derive a different formula in the strong turbulence limit, namely

$$\lambda_\parallel \sim R_L\frac{B_0}{\delta B} \qquad \textit{(Modified Bohm Limit)}. \quad (3)$$

We call this formula the *modified Bohm limit*. In this case the parallel mean free path is still directly proportional to the unperturbed Larmor radius R_L, but is reduced by the factor $\delta B/B_0$. Equation (3) was confirmed analytically in more recent work (see Srinivasan & Shalchi 2014). Formula (3) was derived for the parallel mean free path. Perpendicular diffusion in the strong turbulence limit is another interesting topic. If the turbulence is isotropic and strong, one would expect to see isotropic particle diffusion, i.e., $\lambda_\perp \approx \lambda_\parallel$.

Above we have presented some analytical approaches and results in different physical limits. Another powerful tool in diffusion theory is test-particle simulations, where a certain turbulence model is simulated, and then the *Newton–Lorentz equation* is solved numerically in order to obtain a high number of particle orbits. By using simple methods of statistical physics, one can easily obtain diffusion coefficients from these test-particle trajectories. For different turbulence models and parameters, computer simulations were performed in the past (see, e.g., Giacalone & Jokipii 1999; Michałek 2001; Casse et al. 2002; Qin et al. 2002a, 2002b, 2006; Candia & Roulet 2004; Shalchi 2005; Zimbardo et al. 2006; Tautz 2010; Dosch et al. 2011). It remains unclear what the diffusion parameters are in the strong turbulence limit and whether or not Equation (2) or Equation (3) are correct.

This article will explore numerically the transport of energetic particles along and across the mean magnetic field in the strong turbulence limit. We focus on the testing the Bohm limit, but will also explore how the simulated turbulence model affects the diffusion parameters. It is our aim to explore the validity of the limits (2) and (3).

2. TEST PARTICLE SIMULATIONS

In computer simulations three steps must be performed in order to obtain diffusion parameters, which are listed as follows.

1. A specific turbulence model has to be simulated. Here, we consider the slab model, a combined slab/two-dimensional (2D) model, and the isotropic model.
2. The *Newton–Lorentz equation* has to be solved numerically for an ensemble of particles to obtain their orbits.
3. From these test-particle trajectories, one can easily obtain the diffusion coefficients in the different directions of space.

We will briefly discuss the methods used in the simulations in order to obtain the diffusion coefficients and mean free paths.

2.1. Turbulence Models

As described above, we have to specify the turbulence model. We perform the simulations for three specific models, which are listed as follows.

1. The *slab model* in which by definition $\delta \boldsymbol{B} = \delta \boldsymbol{B}(z)$ (i.e., the turbulent field depends only on the coordinate along the mean field). Furthermore, we have $\delta B_z = 0$ due to the *solenoidal constraint*. This means that in slab turbulence the turbulent field vector is always perpendicular with respect to the mean field.
2. We also consider a *slab/2D composite model* in which we superpose the slab model discussed above with a 2D model in which we have by definition $\delta \boldsymbol{B} = \delta \boldsymbol{B}(x, y)$. Similar to the slab model, the 2D model has reduced dimensionality. However, we still have some choice concerning the allowed magnetic field orientations. Here, we use a full 2D model where we also have $\delta B_z = 0$. This means that the coordinate dependence, as well as the field vector itself, are 2D. Each model has a weight contributing to the total power. In our case we used a mixture proposed by Bieber et al. (1996) based on spacecraft measurements of the interplanetary magnetic field in which a 80% 2D fluctuation and/20% slab fluctuation is obtained.
3. *Isotropic turbulence* in which the turbulence is full isotropic and, therefore, only the mean magnetic field breaks the symmetry of the physical system.

2.2. Generating the Turbulence

The most commonly used technique to generate magnetic turbulence is to sum over a large number of plane waves, N, with random phases, polarization, amplitudes, and orientations. Batchelor (1953) showed that when the number of wave modes tends to infinity, turbulence becomes isotropic and spatially homogeneous. Strictly speaking, in reality, wave-numbers also extend until infinity, but as we are using a numerical approach infinity is out of reach, so the limitation should take place (see below for simulation parameters). Speaking mathematically, turbulent fields are generated as the following summation over the N_m wave modes:

$$\delta \mathbf{B}(x, y, z) = \mathcal{R}e \sum_{n=1}^{N_m} A(k_n) \hat{\boldsymbol{\xi}}_n \exp i(k_n z_n' + \beta_n), \qquad (4)$$

where

$$\hat{\boldsymbol{\xi}_n} = \cos(\alpha_n)\hat{\mathbf{x}}_n' + i \ \sin(\alpha_n)\hat{\mathbf{y}}_n', \qquad (5)$$

denotes the field orientation. The primed notation refers to the turbulence coordinates obtained from a three-dimensional rotational matrix given by

$$\begin{pmatrix} x_n' \\ y_n' \\ z_n' \end{pmatrix} = \begin{pmatrix} \cos\theta_n \cos\phi_n & \cos\theta_n \sin\phi_n & -\sin\theta_n \\ -\sin\phi_n & \cos\phi_n & 0 \\ \sin\theta_n \cos\phi_n & \sin\theta_n \sin\phi_n & \cos\theta_n \end{pmatrix} \begin{pmatrix} x \\ y \\ z \end{pmatrix}. \qquad (6)$$

In Equations (4)–(6) we used $A(k_n)$ to represent the wave amplitude associated with mode n. In addition, k_n stands for the wave-number, α_n for polarization angle, θ_n and ϕ_n define the orientation of mode n, and β_n is the plane wave phase. Note that the static wave's orientation is governed by the following relation:

$$z_n' = \sin\theta_n \cos\phi_n x + \sin\theta_n \sin\phi_n y + \cos\theta_n z. \qquad (7)$$

As presented below, the turbulence model controlled by the choice of angles will restrict the direction. One of the points that should be emphasized here is that turbulent fields are divergence-free (i.e., $\boldsymbol{\nabla} \cdot \delta \mathbf{B} = 0$), as Maxwells' equations predict. This condition is preserved via the relation, $\mathbf{k_n} \cdot \hat{\boldsymbol{\xi}_n} = \mathbf{0}$, since z' (plane waves orientation) is always perpendicular to $\hat{\boldsymbol{\xi}}_n$, as defined above. Isotropic turbulence can be achieved by summing over a high number of wave modes within our simulations, $N = 512$, with all angles θ, ϕ, α, and β chosen randomly and which lie in the interval $[0, 2\pi[$. For the slab model, the orientation of plane waves is the same as the mean field, $z' = z$, so we set $\theta_n = 0$ in Equation (6). On the other hand, the 2D model requires $z' \perp z$ for the turbulent field to only depend on $\hat{\mathbf{x}}$ and $\hat{\mathbf{y}}$ coordinates, hence setting $\theta = \pi/2$ is sufficient. This paper is restricted to working with a full 2D model as presented above (i.e., having $\delta B_z = 0$ or $\delta \mathbf{B} \perp \hat{\mathbf{z}}$), so an additional condition should be added, where we set the polarization angle $\alpha = \pi/2$.

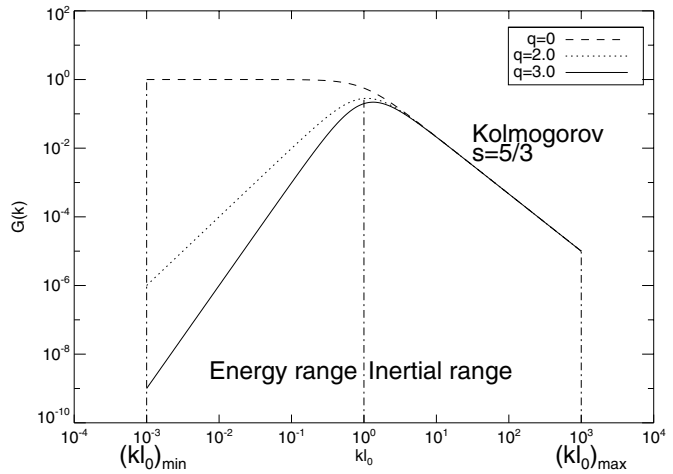

Figure 1. Spectrum for slab, composite, and isotropic turbulence with respective values of $q = 0.0,\ 2.0,$ and 3.0 over a spread of wave-numbers ranging from $k_{\rm min}l_0 = 10^{-3}$ to $k_{\rm max}l_0 = 10^3$ in dimensionless units. At $kl_0 = 1$, a transition from energy to inertial range takes place.

Another ingredient in the description of turbulence is the turbulence power spectrum, which describes how the magnetic energy is distributed among different wave numbers. The different spectra used in this paper are visualized in Figure 1. They are based on the model originally proposed by Shalchi & Weinhorst (2009), and are usually divided into different ranges. The larges scales are usually referred to as the *energy range* and the intermediate scales are called the *inertial range*. The characteristic length scale where the turnover from the energy range to the inertial range occurs is usually called the *bendover scale*. One could also add a so-called *dissipation range* describing the small scales. This regime, however, is only important for very low energy particles and we do not investigate this type of transport in the current paper. In the energy range we assume a power-law dependence of the magnetic fluctuation with k^q, where q is called the *energy range spectral index*. In the inertial range we also assume a power-law with k^{-s}, where s is the *inertial range spectral index*. Whereas one usually assumes that $s = 5/3$ in agreement with the theory of Kolmogorov (see Kolmogorov 1941), the value of q is unknown. Therefore we use different values for the energy range spectral index. Below we use $q = [0.0, 2.0, 3.0]$ for slab, 2D, and isotropic turbulence, respectively.

Mathematically speaking, the wave amplitude $A(k_n)$ reads

$$A^2(k_n) = G(k_n)\Delta k_n \left(\sum_{\eta=1}^{N_m} G(k_\eta)\Delta k_\eta \right)^{-1}, \tag{8}$$

where the turbulence spectrum is defined as a *Kappa-type* form continuously differentiable:

$$G(k_n) = \frac{k_n^q}{\left(1 + k_n^2\right)^{(s+q)/2}}. \tag{9}$$

Δk_n is the spacing between wave-numbers, where a logarithmic spacing in k_n is implemented so that $\Delta k_n / k_n$ is constant via the relation

$$\frac{\Delta k_n}{k_n} = \exp\left[\frac{ln(k_{\rm max}/k_{\rm min})}{N-1} \right]. \tag{10}$$

Figure 1 shows the turbulence spectrum we use for the three different turbulence models (slab, composite, and isotropic). There are two main constraints that should be taken into account for each simulation. First, what is known by the resonance condition ensuring the existence of a wave-number satisfying the relation $k\mu R_L = 1$. Here μ is the pitch-angle cosine and R_L is the unperturbed Larmor radius defined as $R_L = pc/eB_0 = Rl_0$ where R is the dimensionless rigidity. This constraint is ensured as $\mu \in [-1, 1]$, $kl_0 \in [10^{-3}, 10^3]$, and $R = [0.1, 1, 10]$. We also ensure that no particle is traveling more than the distance $L_{\rm max} = k_{\rm min}^{-1}$. This is ensured via the relation $\Omega t_{\rm max} k_{\rm min} R_L < 1$, which corresponds to $vt_{\rm max} < L_{\rm max}$.

2.3. Solving the Newton–Lorentz Equation

The Newton–Lorentz equation for a particle in purely magnetic turbulence reads

$$\dot{\boldsymbol{p}} = \frac{q}{c}\boldsymbol{v} \times \boldsymbol{B}\left[\boldsymbol{x}(t), t\right], \tag{11}$$

where $\boldsymbol{x}(t)$ is the position of the charged particle. Furthermore, we used the particle charge q, the speed of light c, the particle velocity $\boldsymbol{v}$, and the (relativistic) momentum $\boldsymbol{p} = m\gamma\boldsymbol{v}$, where γ is the *Lorentz factor*. Our code uses a Monte Carlo method where each particle injected has a different and random initial set of parameters. Initially, all particles have the same z-coordinate and energy value. However, their initial x and y coordinates and values of the pitch-angle cosine μ are different. The particles are traced for a fairly sufficient time for thousands of gyro-periods in order to precede the initial ballistic regime in which the particle's diffusion coefficient is linearly proportional to time. There are two ways to implement the generated magnetic fields in such codes.

1. *Using discrete grid.* With grid systems we first create and save the fields data at each grid point using Equations (4)–(10) for the whole space and then interpolate for where the particle is moving. This could be done using a 2D grid for the perpendicular directions, accompanied with a one-dimensional grid for the parallel direction, or rigorously using a three-dimensional grid (see, for example, Mace et al. 2000; Qin et al. 2002a; Casse et al. 2002; Pommois et al. 2007; Reville et al. 2008).
2. *Creating fields along the trajectory.* Fields are generated anew at each time step where it is needed using the same set of equations. Fields are generated anew at each time step. With the known initial position of the particle, we can compute the initial magnetic field vector. The latter quantity is then seeded to the numerical integrator to solve for position which is then seeded to turbulence creation and so on (see, e.g., Giacalone & Jokipii 1999; Tautz 2010; Dosch et al. 2011).

Each method has pros and cons concerning time consumption, memory usage, and accuracy. Based on previous experience with grid points codes, it seems to us that the second method is better than the first. It saves time, uses less memory (given that too many grid points must be used to achieve acceptable accuracy), and it generates fields only where the particle is actually moving, not on all the provided space as the first method does. On the other hand, when it comes to visualization, the grid-based system allows us to visualize the magnetic field lines across the whole space and then see how the particles are moving in the vicinity of those field lines, whereas with the method we are using this is not possible, as magnetic information is restricted for where particles are moving.

The numerical solver used to integrate the *Newton–Lorentz equation* is *Runge–Kutta* of 4th order with an adaptive time-step option based on calculating the gyro-frequency, $\Omega = qB_0/\gamma mc$, where B_0 is the background field, and multiplying its inverse by a point-one factor to keep truncation errors under control. To allow for generality of the code parameters were made dimensionless so we define the characteristic length, known as the turbulence bendover scale, l_0, for which the position parameters are scaled to. In addition, l_0 denotes the turnover from the energy to the inertial range (see Figure 1), where estimates of solar system bendover scale is around $l_0 = 0.03$ AU. The relativistic gyro-frequency is the inverse of the characteristic time, hence we could define the (dimensionless) running time as $\tau = \Omega t = qB_0 t/\gamma mc$. Dimensionless rigidity is given by, $R = R_L/l_0 = v/\Omega l_0$. Given those dimensionless parameters, one can derive the numerically solved dimensionless *Newton–Lorentz equation*, coupled with the trajectory equation, as follows:

$$\frac{d}{d\tau}\frac{\mathbf{x}}{l_0} = \mathbf{R}, \tag{12}$$

$$\frac{d}{d\tau}\mathbf{R} = \mathbf{R} \times \left(\hat{\boldsymbol{e}}_{B_0} + \frac{\delta B}{B_0}\hat{\boldsymbol{e}}_{\delta B}\right) \tag{13}$$

where $\hat{\boldsymbol{e}}_{B_0}$ and $\hat{\boldsymbol{e}}_{\delta B}$ denote the unit vectors pointing in the direction of the background and turbulent magnetic fields, respectively. Note that the code implements the concept of turbulence strength, $\delta B/B_0$, directly in the solved equation.

2.4. Calculating the Transport Parameters

If the particle trajectories are obtained numerically, the remaining step is the calculation of the diffusion coefficient. Often diffusion coefficients are computed using mean square displacements:

$$\kappa_{ii} = \lim_{t\to\infty} \frac{1}{2}\frac{d}{dt}\langle(\Delta x_i)^2\rangle. \tag{14}$$

This formula, however, cannot be used if it comes to the *drift coefficient* κ_{xy} (see Shalchi 2011). Alternatively, one can compute the diffusion parameter with

$$\kappa_{ii} = \lim_{t\to\infty} \langle \Delta x_i v_i \rangle \tag{15}$$

which avoids the usage of derivative operators. In the present paper we compute mean free paths, defined as

$$\lambda_i = 3\kappa_i/v \tag{16}$$

because the latter parameter has more appropriate units (i.e., we can compute the ratio λ_i/l_0, where l_0 is the characteristic length scale of the turbulence).

3. RESULTS

3.1. Simulation Parameters

We choose three values of particle rigidity $R \in [0.1, 1.0, 10.0]$. For each rigidity, we perform simulations for the five different values of turbulence strength $\delta B/B_0 \in [0.1, 1.0, 10.0, 50.0, 100.0]$, and we consider three different turbulence models, namely slab, composite, and isotropic turbulence. Therefore, we have 45 simulations in total.

The trajectories of 1000 particles were traced for a sufficient dimensionless time, $\tau_{\max} = \Omega t_{\max} = 10^4$, and averaged using 1000 Realization, which means that every particle has its own set of initializing parameters, mainly turbulence angles, supported by the high efficiency and the processor capacity provided by *WestGrid National Facility*. This feature allows for more accuracy compared to similar previous works, given that in reality each particle sees the turbulence from its perspective. We used $N_m = 512$ different wave modes to create turbulence at each time step, which is enough to achieve isotropic conditions with wave-numbers in the coordinates x, y, and z, ranging from $k_{\min} l_0 = 10^{-3}$ to $k_{\max} l_0 = 10^3$ in dimensionless units. The energy range, q, as presented above, differs with respect to the turbulence model. The Kolmogorov (1941)-like inertial range is the same for all models, namely $s = 5/3$.

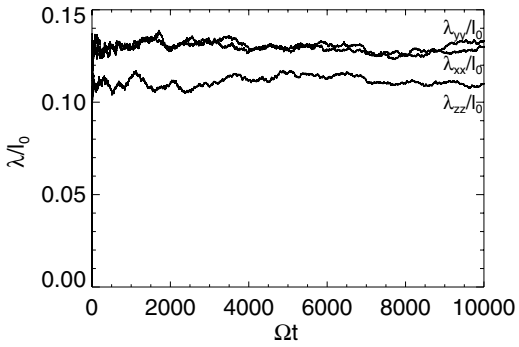

Figure 2. Mean free paths λ_{xx}/l_0, λ_{yy}/l_0, and λ_{zz}/l_0 for $R = 10.0$ and $\delta B/B_0 = 100$ vs. Ωt.

3.2. The Parallel Mean Free Path

Our main focus in this paper is to check the validity of the modified Bohm limit for strong turbulence. The validity of the standard Bohm limit was explored before (see, e.g., Dosch et al. 2011), but due to the too low achievable maximum turbulence strength, no conclusion was obtained for the particle transport in the strong turbulence limit. In such previous work the maximum was $(\delta B/B_0)^2 = 10$, whereas in our work we reach up to $(\delta B/B_0)^2 = 10^4$. Figure 2 shows the mean free paths in the different directions in space for $R = 10.0$, $\delta B/B_0 = 100$, and isotropic turbulence. Our proposed formula, Equation (3), predicts a value of $\lambda_\parallel/l_0 = 0.1$, and using an isotropic model at high turbulence we anticipate that $\lambda_{xx} = \lambda_{yy} = \lambda_\perp \sim \lambda_\parallel$. From Figure 2 it can be determined that $\lambda_\parallel/l_0 \simeq 0.11$, $\lambda_{xx}/l_0 \sim \lambda_{yy}/l_0 \simeq 0.13$, and the diffusive behavior is obvious, which matches with our expectations.

Figures 3–5 show the parallel mean free path $\lambda_\parallel/l_0$ versus the turbulence strength $\delta B/B_0$ for $R = 0.1$, 1.0, and 10.0, respectively. In all the figures we have shown the results for slab, composite, and isotropic turbulence.

We clearly show that the well-known and widely used standard Bohm limit, Equation (2), is not valid. It seems that the modified limit, Equation (3), is indeed the correct lower limit for the parallel diffusion coefficient. One of the interesting values to plot is $\lambda_\parallel/R_L$ versus R_L, leaving the factor $B_0/\delta B$ on the other side of the equation, such that $\lambda_\parallel/R_L \sim B_0/\delta B$. Figures 6–8 show the results for slab, composite, and isotropic turbulence, respectively. Shalchi (2005) performed similar simulations with particles of rigidity $R = 0.1$ and a composite turbulence model of strengths ranging from 0.5 to 100 and calculated values of $\lambda_\parallel/l_0$, $\lambda_\perp/l_0$, and $\lambda_\perp/\lambda_\parallel$. The author did not compare his simulations with the standard Bohm limit and the modified limit did not exist at that time. In Figure 3 we plotted those results

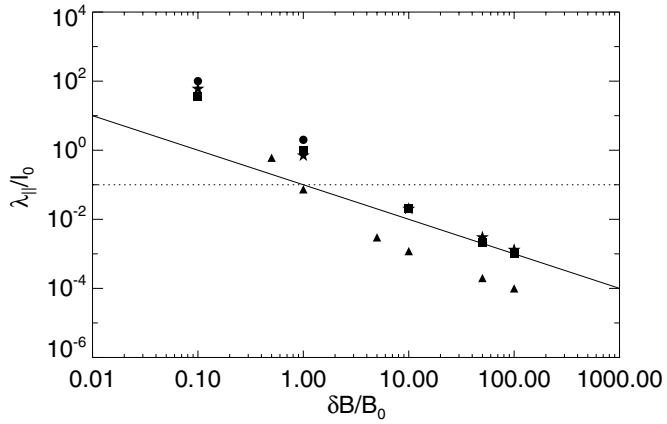

Figure 3. $\lambda_\parallel$ normalized to the bendover length l_0 vs. turbulence strength $\delta B/B_0$ for low energetic particles $R = 0.1$. The plot also shows $\lambda_\parallel/l_0$ for the three different models (slab, composite, and isotropic), plotted as circles, squares, and stars, respectively. The dashed lines represent the standard Bohm limit with $\lambda_\parallel \sim R_L$, whereas the solid lines indicate the modified Bohm limit where $\lambda_\parallel \sim R_L B_0/\delta B$. Triangles represent the Shalchi (2005) simulations.

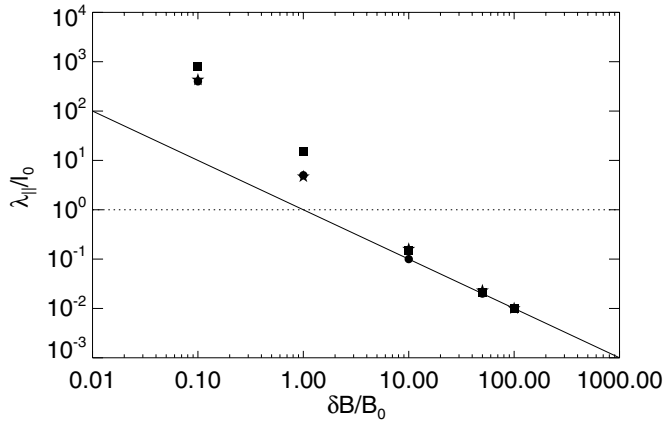

Figure 4. Same as Figure 3, but for intermediate particle rigidities with $R = 1.0$.

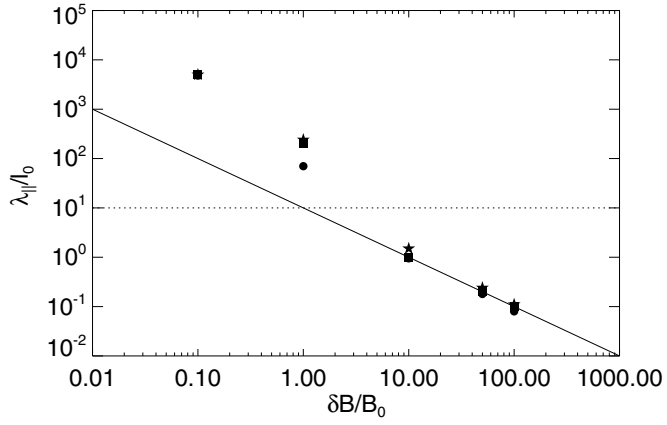

Figure 5. Same as Figure 3, but for high particle rigidities with $R = 10.0$.

for comparison. Despite the fact that the Shalchi (2005) results overcome the Bohm limit, it seems, that the general behavior of $\lambda_\parallel/l_0$ in both simulations is similar.

3.3. The Perpendicular Mean Free Path

In the following we discuss the perpendicular diffusion coefficient. Here we only consider axi-symmetric turbulence, and, therefore, we have $\kappa_\perp = \kappa_{xx} = \kappa_{yy}$. Previous works with

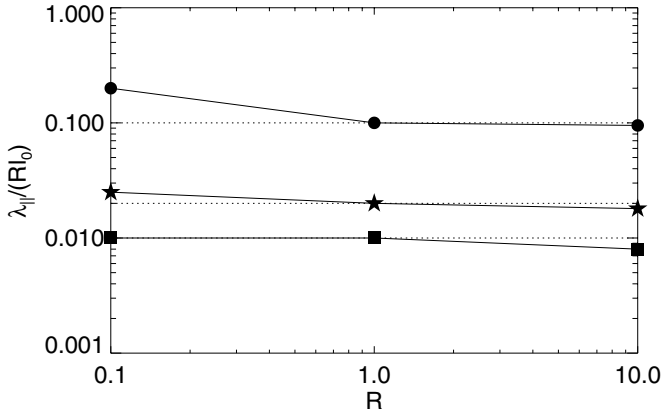

Figure 6. $\lambda_\parallel/(Rl_0)$ vs. R for $\delta B/B_0 = 10.0,\ 50.0,$ and 100.0 plotted as circles, stars, and squares, respectively, for the slab model validating the relation of $\lambda_\parallel/(Rl_0) \sim B_0/\delta B$. Dashed lines from top to bottom correspond to the right hand side of the latter relation, that is $B_0/\delta B = 0.1,\ 0.02,$ and 0.01.

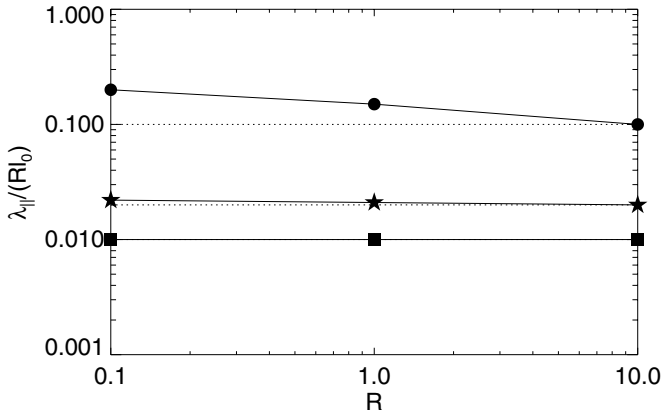

Figure 7. Same as in Figure 6, but for composite turbulence.

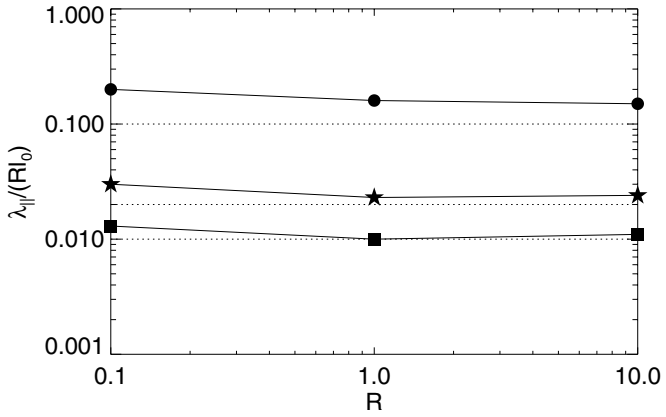

Figure 8. Same as in Figure 6, but for isotropic turbulence.

a maximum turbulence strength of $(\delta B/B_0)^2 = 10$ showed that $\lambda_\perp/l_0$ is linear in R (see, e.g., Giacalone & Jokipii 1999; Qin 2002; Tautz et al. 2006). Furthermore, Giacalone & Jokipii (1999) showed that $\kappa_\perp$ is linear in $\delta B/B_0$, but the author's maximum strength was $\delta B = B_0$. In our simulations we recovered the previous results, which could be regarded as intermediate turbulence, and revealed what happens when turbulence is extremely strong. Figures 9 and 10 show $\lambda_\perp/l_0$ versus R and $\delta B/B_0$, respectively, for both composite and isotropic turbulence. As shown there, $\lambda_\perp/l_0$ remains linear in R for both composite and isotropic turbulence. The dependence on $\delta B/B_0$ is more complicated. For composite turbulence, the

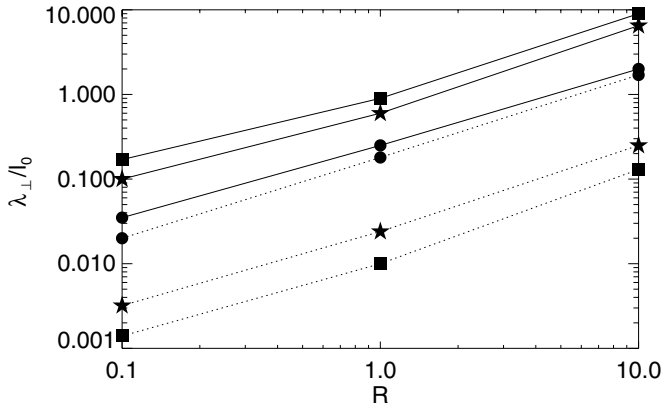

Figure 9. Perpendicular mean free path, $\lambda_\perp$, normalized to l_0 with respect to rigidity R for high turbulence scenarios of $\delta B/B_0 = 10, 50,$ and 100, plotted as circles, stars, and squares, respectively, for composite (solid lines) and isotropic (dashed lines) models.

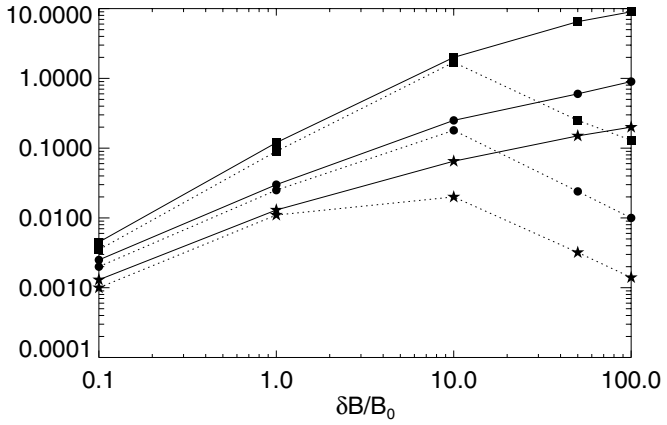

Figure 10. $\lambda_\perp/l_0$ vs. $\delta B/B_0$ for the three different particles of $R = 0.1$, 1.0, and 10.0 plotted as stars, circles, and squares, respectively, for composite (solid lines) and isotropic (dashed lines) models.

perpendicular mean free path increases linearly with $\delta B/B_0$. For isotropic turbulence, however, it increases in the weak turbulence regime and decreases in the strong turbulence regime.

Figure 11 shows $\lambda_\perp/\lambda_\parallel$ versus $\delta B/B_0$ for $R = 0.1$ for both composite and isotropic turbulence. For the sake of comparison we also show the results obtained by Shalchi (2005) for composite turbulence. It seems that in the weak turbulence regime, $\lambda_\perp/\lambda_\parallel$ is $\propto (\delta B/B_0)^\alpha$, where α is $\approx$3.1 and 3.3 for composite and isotropic turbulence, respectively. For strong turbulence we can see a clear deviation between the results obtained for composite and isotropic turbulence. For the former case the ratio $\lambda_\perp/\lambda_\parallel$ still increases with $\delta B/B_0$, but α drops to values around 2. Furthermore, we find that $\lambda_\perp/\lambda_\parallel$ exceeded unity, which corresponds to previous observations (see Zhang et al. 2003 and Dwyer et al. 1997). Despite a numerical factor at weak turbulence, our results for $\lambda_\perp/\lambda_\parallel$ agree well with Shalchi (2005). For strong isotropic turbulence, we find $\lambda_\perp \approx \lambda_\parallel$ as expected.

4. SUMMARY AND CONCLUSION

Here we have revisited an important and fundamental topic in astrophysics, namely the transport of energetic particles such as cosmic rays. We used a test-particle method to compute diffusion coefficients along and across the mean magnetic field. Our main aim was to explore the validity of the *Bohm limit*, but

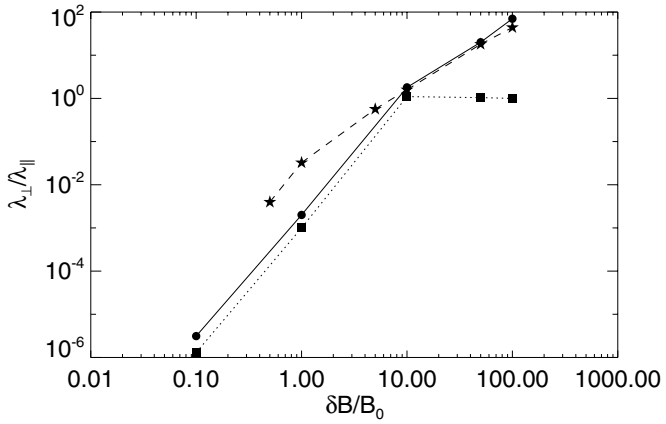

Figure 11. $\lambda_\perp/\lambda_\parallel$ vs. $\delta B/B_0$ for composite (circles) and isotropic (squares) models. The case considered refers to low energetic particles with $R = 0.1$. Shalchi (2005) results are plotted as stars for comparison.

we also investigated the influence of the turbulence model on the transport.

In previous works, researchers used the standard Bohm limit in which we have $\lambda_\parallel \approx R_L$, where R_L is the unperturbed Larmor radius. Particularly in investigations of diffusive shock acceleration at supernova shocks, the assumption of Bohm diffusion seems to be standard (see, e.g., Berezhko & Völk 1997; Uchiyama et al. 2007; Jones 2011; Bell et al. 2013). However, the standard Bohm limit disagrees with the limit derived in Shalchi (2009b) and Srinivasan & Shalchi (2014) where the formula $\lambda_\parallel \approx R_L B_0/\delta B$ is obtained for the parallel mean free path in the strong turbulence limit (here we have omitted numerical factors). We have shown here that the simulated parallel mean free path can be much shorter than the unperturbed Larmor radius and, therefore, the limit $\lambda_\parallel \approx R_L$ is not correct. Furthermore, we did not find any evidence that the latter formula is valid in a certain parameter regime. Is seems, however, that the formula $\lambda_\parallel \approx R_L B_0/\delta B$ is indeed correct in the limit of strong turbulence. We have shown that extremely strong turbulence is needed in order to get close to this formula.

We have also obtained perpendicular diffusion coefficients from our simulations. $\lambda_\perp/l_0$ seems to be directly proportional to rigidity R regardless of the turbulence model or strength. If one computes $\lambda_\perp/l_0$ versus $\delta B/B_0$, however, the isotropic and composite results are different in the strong turbulence regime. In the former case, one finds isotropic scattering with $\lambda_\perp \approx \lambda_\parallel$ as expected. For composite turbulence, the perpendicular mean free path increases with $\delta B/B_0$. In this particular regime the influence of the turbulence model is crucial.

M. Hussein and A. Shalchi acknowledge support by the Natural Sciences and Engineering Research Council (NSERC) of Canada and national computational facility provided by WestGrid. We are also grateful to Samar Safi-Harb for providing her CFI-funded computational facilities for code tests and for some of the simulation runs presented here.

REFERENCES

Batchelor, G. K. 1953, The Theory of Homogeneous Turbulence (Cambridge: Cambridge Univ. Press)
Bell, A. R., Schure, K. M., Reville, B., & Giacinti, G. 2013, MNRAS, 431, 415
Berezhko, E. G., & Völk, H. J. 1997, APh, 7, 183
Bieber, J. W., Wanner, W., & Matthaeus, W. H. 1996, JGR, 101, 2511
Candia, J., & Roulet, E. 2004, JCAP, 10, 007
Casse, F., Lemoine, M., & Pelletier, G. 2002, PhRvD, 65, 023002

Dosch, A., Shalchi, A., & Tautz, R. C. 2011, MNRAS, 413, 2950
Dwyer, J. R., Mason, G. M., Mazur, J. E., et al. 1997, ApJL, 490, L115
Giacalone, J., & Jokipii, J. R. 1999, ApJ, 520, 204
Jokipii, J. R. 1966, ApJ, 146, 480
Jones, T. W. 2011, JApA, 32, 427
Kolmogorov, A. 1941, DoSSR, 30, 301
Mace, R. L., Matthaeus, W. H., & Bieber, J. W. 2000, ApJ, 538, 192
Michałek, G. 2001, A&A, 376, 667
Pommois, P., Zimbardo, G., & Veltri, P. 2007, PhPl, 14, 012311
Qin, G. 2002, PhD thesis Univ. of Delaware
Qin, G., Matthaeus, W. H., & Bieber, J. W. 2002a, ApJL, 578, L117
Qin, G., Matthaeus, W. H., & Bieber, J. W. 2002b, GeoRL, 29, 7
Qin, G., Matthaeus, W. H., & Bieber, J. W. 2006, ApJL, 640, L103
Reville, B., O'Sullivan, S., Duffy, P., & Kirk, J. G. 2008, MNRAS, 386, 509
Schlickeiser, R. 2002, Cosmic Ray Astrophysics (Berlin: Springer)
Schlickeiser, R., Dohle, U., Tautz, R. C., & Shalchi, A. 2007, ApJ, 661, 185
Shalchi, A. 2005, MNRAS, 363, 107
Shalchi, A. 2009a, Nonlinear Cosmic Ray Diffusion Theories, Astrophysics and Space Science Library, Vol. 362 (Berlin: Springer)
Shalchi, A. 2009b, APh, 31, 237
Shalchi, A. 2010, ApJL, 720, L127
Shalchi, A. 2011, PhRvE, 83, 046402
Shalchi, A., & Weinhorst, B. 2009, AdSpR, 43, 1429
Srinivasan, S., & Shalchi, A. 2014, Ap&SS, 350, 197
Tautz, R. C. 2010, CoPhC, 181, 71
Tautz, R. C., Shalchi, A., & Schlickeiser, R. 2006, JPhG, 32, 809
Uchiyama, Y., Aharonian, F. A., Tanaka, T., Takahashi, T., & Maeda, Y. 2007, Natur, 449, 576
Zhang, M., Jokipii, J. R., & McKibben, R. B. 2003, ApJ, 595, 493
Zimbardo, G., Veltri, P., & Pommois, P. 2006, ApJL, 639, L91